ELSEVIER

International Journal of Heat and Fluid Flow 19 (1998) 601–607

International Journal of HEAT AND FLUID FLOW

Three-dimensional flow in axial flow fans of non-free vortex design

János Vad, Ferenc Bencze *

Department of Fluid Mechanics, Technical University of Budapest, Bertalan Lajos u. 4-6, 1111 Budapest, Hungary

Received 12 July 1997; accepted 21 February 1998

Abstract

Three-dimensional laser Doppler anemometer (LDA) measurements were carried out downstream of isolated axial fan rotors of non-free vortex design in order to investigate the role of radial velocity components in design. The structure of secondary flows due to non-free vortex operation was studied in detail. It is pointed out that the tangential gradient of radial velocity at midspan is nearly in direct proportion with the spanwise gradient of ideal total head rise prescribed in design. Design criteria have been established for the neglect of torsion of stream surface segments inside the blading. A linear relationship was proposed in order to estimate the pitch-averaged radial velocities at the rotor exit. Using this relationship, a proposal has been put forward for taking the radial velocity components into account in non-free vortex design with the assumption of conical stream surfaces through the blading.

Keywords: Laser Doppler anemometry; Axial flow fan; Non-free vortex design; Three-dimensional flow; Secondary flow

Notation

c	absolute velocity
c_{lift}	lift coefficient
ℓ	blade chord
n	design power exponent
N	blade number
r	radius
$R = r/r_c$	dimensionless radius
$R_{\text{mid}} = (1+\nu)/2$	midspan radius
ΔR	radial deviation
$t = 2r\pi/N$	blade pitch
T	passing time
u_c	reference velocity ($r_c\omega$)
w	relative velocity
α_{cone}	conical stream surface half-angle
γ	blade stagger angle (measured from the circumferential direction)
δ	stream surface torsion angle (see Fig. 5)
θ	angular co-ordinate (central angle, see Fig. 5)
$\overline{\Phi}$	flow coefficient (area-averaged axial velocity in the annulus divided by u_c)
$\varphi_3 = c_{3x}/u_c$	local axial flow coefficient
$\varphi_{r3} = c_{3r}/u_c$	local radial flow coefficient
$\psi_3 = 2\,R\,c_{3u}/u_c$	local ideal total head rise coefficient (assuming zero inlet swirl)
$\overline{\Psi}_t$	average total head rise coefficient (total head rise in the annulus normalised by $\rho u_c^2/2$)
ρ	fluid density
ν	hub-to-casing ratio
τ	average tip clearance
ω	rotor angular speed
η_h	hydraulic efficiency

Subscripts and superscripts

c	casing wall
D	design
r, u, x	radial, tangential, axial
0	rotor inlet plane
3	rotor exit plane
∞	isolated airfoil characteristic
$\wedge$	pitch-averaged
*	theoretical flow data (corresponding to two-dimensional stationary cascade measurements)

1. Introduction

If high average total head rise is to be achieved with relatively low blade number, rotor speed and hub-to-casing ratio, the non-free vortex axial fan rotor design method (abbr. NFV method) is applied. In NFV design, a spanwise increasing ideal total head rise is prescribed.

A number of NFV methods are based on two-dimensional cascade measurements, neglecting the radial velocity components and thus, assuming cylindrical stream surfaces through the blading (Wallis, 1961; Somlyódy, 1971; Bencze and Szlivka, 1987). However, it is well known that the spanwise gradient in ideal total head rise results in development of a three-dimensional secondary flow (abbr. NFVO flow for

* Corresponding author. E-mail: bencze@goliat.eik.bme.hu.

0142-727X/98/$ – see front matter
PII: S0142-727X(98)10004-8

"Flow due to Non-Free Vortex Operation") inside the blade passages. Computations by Wu (1952) illustrate that the cylindrical inlet stream surfaces are split by the rotating cascade and the resultant stream surface segments are shifted and twisted by the blading. The appearance of radial velocities raises the following design questions: (i) Is the torsion of stream surface segments negligible? In other words: is the assumption of stream surfaces of revolution reasonable? (ii) If so, are the pitch-averaged radial velocities negligible, i.e. is the assumption of cylindrical stream surfaces reasonable?

To provide data on radial flow effects, several calculations have been carried out (e.g. Dodge, 1976; Briley and McDonald, 1979; Caspar et al., 1980), which necessitated experimental data for comparison.

Generally speaking, only a few experimental results have been published on rotors of NFV design. Though measurements by Meixner (1994) were aimed at such rotors, they were confined to the axial and tangential velocity components, not making possible the study of radial flow. Work by Dring et al. (1982) deals apparently with a rotor of NFV design, however, the paper does not contain sufficient information on the applied rotor design method. Some papers publish measurement results on rotors of non-free vortex operation generated by off-design conditions (Wagner et al., 1985; Goto, 1992). In such cases, the off-design operation may result in undesirable phenomena, e.g. thickened or separated blade boundary layers, which make the application of the measured radial flow data doubtful in NFV design. On the other hand, the measurement data usually concern only one rotor in each of the references, which also limits their application in general design.

This paper provides information on the radial flow developing in a family of rotors of NFV design, in order to reduce the above discussed lack in experimental data and to supply instructions for the design consideration of radial velocity components. The study is based on three-dimensional LDA measurements carried out downstream of the rotors.

2. Experimental facility, instrumentation and measurement error

The experimental program was carried out in the axial flow fan facility at the Department of Fluid Mechanics, Technical University of Budapest. The facility, instrumentation and measurement method is described in detail in Vad et al. (1995) and Vad and Bencze (1996) so only a brief account is given here. A long inlet section with an inlet cone and honeycombs precedes the working section which has a 0.630 m outer dia and hub-to-casing ratio $\nu = 0.676$. Prerotator and straightener blades can be installed if necessary. Far downstream of the rotor is an outlet diffuser and a throttle to the atmosphere. The facility is capable for automatic efficiency and characteristic curve measurements.

The three rotors on investigation, designated with BUP-26, BUP-29 and BUP-103, are characterised with the following common parameters: $N = 12$ straight (unswept) circular arc plate blades, design flow coefficient $\bar{\Phi}_D = 0.5$, average tip clearance $\tau = 3$ mm. They were run at a speed of 1100 rpm. The aerodynamic design, proposed by Somlyódy (1971), assumes a uniform axial inlet flow and prescribes a power function ideal total head rise distribution along the radius

$$\hat{\psi}_{3D}|_R = \hat{\psi}_{3D}|_{R=\nu}\left(\frac{R}{\nu}\right)^n. \quad (1)$$

Power exponents n are 1.2, 1.4 and 1.6 for BUP-26, BUP-29 and BUP-103, respectively. By the design conception, the increase in the n exponents makes possible an increase in the average total head rise coefficients at the design flow rate. Furthermore, the growing n values also increase the spanwise gradients in ideal total head rise. The design procedure supplies distributions of $\hat{\varphi}_{3D}(R)$ as well.

In the reported cases, the $\hat{\psi}_{3D}(R)$ distribution by Eq. (1) can be approximated as a linear function with a relative error of less than 5%, due to the relatively high hub-to-casing ratio. This means that the spanwise gradient of $\hat{\psi}_{3D}$ will be characterised along the entire radius by the value of $\partial\hat{\psi}_{3D}/\partial R$ at midspan. Such linearisation was also found admissible for the $\hat{\varphi}_{3D}(R)$ distributions.

The optimum cascade geometry (solidity, chamber radius of curvature and stagger angle) was calculated along the radius assuming cylindrical stream surfaces through the rotor, with the application of the classic method described in Wallis (1961) after Howell (1942). However, the optimum ℓ/t values were realised only at the hub and the corresponding ℓ blade chords (136, 171 and 204 mm for BUP-26, BUP-29 and BUP-103, respectively) were kept constant with span, for simplification in manufacturing. Away from the hub, this compromise resulted in a reduction in solidity relative to the optimum values calculated in advance. At the blade tip, the reduction has relative values of 0.001, 0.133 and 0.272 for BUP-26, BUP-29 and BUP-103, respectively. The details of the airfoil geometries and further design parameters are given in Table 1.

A single-component LDA system is connected to the fan facility. A measurement method has been elaborated for three-dimensional non-simultaneous LDA measurements downstream of the rotors, as summarised in Vad et al. (1995).

The LDA measurements reported here were performed with isolated rotors, i.e. no prerotator or straightener blades were installed. The three-dimensional flow field downstream of the rotors was probed in planes perpendicular to the duct axis. A schematic of the flow path is shown in Fig. 1, indicating the location of the measurement planes.

The flow field downstream of one selected blade passage was measured from hub-to-tip. The central angle of the annular sector measurement region was set to 35° (1 1/7 pitch) to measure one blade wake region contiguously and to check the

Table 1
Rotor airfoil geometry and design parameters

Rotor: BUP-26	Blade root	Midspan	Blade tip
R	0.676	0.833	0.990
$\hat{\varphi}_{3D}$	0.430	0.495	0.561
$\hat{\psi}_{3D}$	0.446	0.578	0.714
(ℓ/t)	1.219	0.984	0.833
Chamber radius/mm	318.0	396.2	480.3
γ/deg	46.8	40.5	36.2
Rotor: BUP-29			
R	0.676	0.833	0.990
$\hat{\varphi}_{3D}$	0.419	0.494	0.573
$\hat{\psi}_{3D}$	0.492	0.665	0.852
(ℓ/t)	1.534	1.237	1.047
Chamber radius/mm	360.7	425.5	493.1
γ/deg	47.9	42.2	38.3
Rotor: BUP-103			
R	0.676	0.833	0.990
$\hat{\varphi}_{3D}$	0.410	0.493	0.581
$\hat{\psi}_{3D}$	0.529	0.747	0.991
(ℓ/t)	1.830	1.476	1.249
Chamber radius/mm	397.4	441.4	486.3
γ/deg	48.8	44.0	40.5

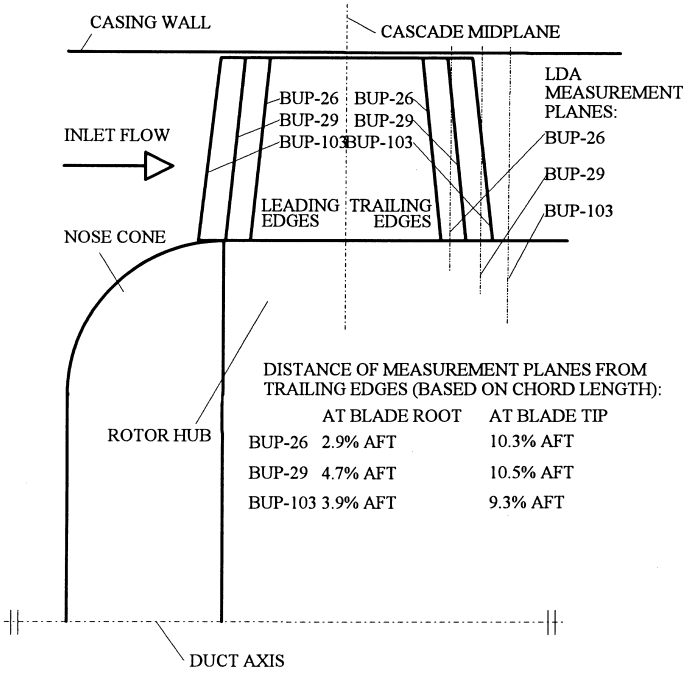

Fig. 1. Flow path schematic and measurement planes.

periodicity in measurement results. Considering the length of LDA probe volume (3 mm) and uncertainty of angular data readout (0.15°), the measurement range was resolved to cells of 5.0% blade height (5.0 mm) in radial direction and 3.3% pitch (1.0°) in circumferential direction. The three velocity components were determined from the ensemble averages of 3×100 LDA data for each cell.

Flow tracking capability calculations have been carried out for the LDA seeding droplets, modelling the relative flow within the blade passage as a decelerating flow in a rotating diffuser. The maximum relative bias error due to droplet lag is 2.5% in tangential, 0.1% in axial velocity and the absolute error in radial velocity is 0.001 u_c. The geometrical misalignments and mechanical deformations cause velocity bias errors. Such errors were estimated through error propagation calculations with the differentiation of the geometrical relationships of the non-orthogonal, non-simultaneous measurement method. These calculations gave a maximum relative error of 1% in tangential, 0.5% in axial velocity and an absolute error of 0.002 u_c in radial velocity. The fluctuation of rotor speed and air density as well as the finite number of LDA data and uncertainties by the data acquisition system caused random errors, which were estimated to a maximum relative error of 2% in tangential and 1.3% in axial velocity. Based on the above details, the LDA experimental uncertainty is estimated as summarised in Table 2.

Table 2
General uncertainty of the presented measurements

	c_u	c_x	c_r
Bias limit (relative error × 100)	3.5	0.6	0.3 [a]
Precision limit (relative error × 100)	2.0	1.3	0.1 [a]
Uncertainty (relative error × 100)	4.1	1.5	0.32 [a]

[a] Absolute error, based on (u_c/100).

3. Overall performance

Fig. 2 shows the performance of the rotors with stator. Considering the $\hat{\psi}_{3D}$ data in Table 1, it is apparent that the overall increase in the $\hat{\psi}_{3D}$ values yields a considerable increase in $\overline{\Psi}_t$ at the design flow rate $\overline{\Phi}_D = 0.5$ for BUP-29 compared to BUP-26. Nevertheless, a further increase in $\hat{\psi}_{3D}(R)$ (BUP-103, compared to BUP-29) seems to be much less effectual from the above viewpoint. Furthermore, it can be observed that BUP-29 has the highest hydraulic efficiency at $\overline{\Phi}_D = 0.5$ and also over a wide surrounding flow rate range.

These observations suggest that BUP-29 behaves the most advantageously among the three rotors from the viewpoints of NFV design concept realisation (considerably increased $\overline{\Psi}_t$) and energy efficiency as well. In Section 4, the reasons of this

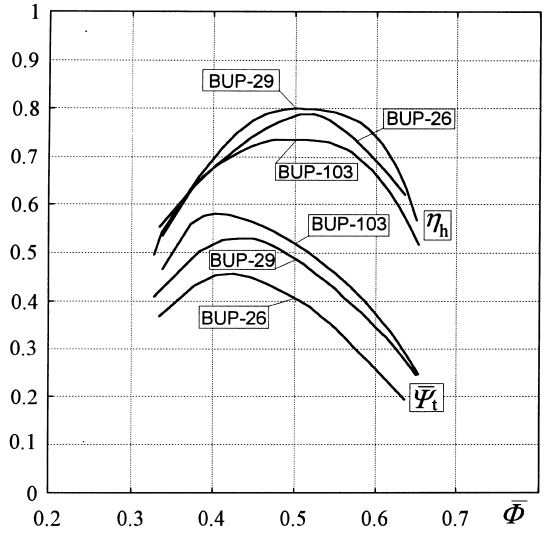

Fig. 2. Fan characteristic and efficiency curves.

special behaviour are investigated through the LDA measurement results.

4. LDA measurement results and discussion

4.1. Pitch-averaged results

During the LDA measurements, the rotors were operated at their design flow rate of $\overline{\Phi}_D = 0.5$. The Reynolds numbers (based on the airfoil chord length and relative inlet flow speed at midspan) were 3.2×10^5, 4.0×10^5 and 4.8×10^5 for BUP-26, BUP-29 and BUP-103, respectively.

A deficiency in the present study is the lack of inlet flow data. We refer to Meixner (1994) who measured the upstream axial velocity profiles for fans of non-free vortex design. The nose cone of the fans studied by Meixner (1994) is similar in geometry to the one shown in Fig. 1. The axial uniform inlet condition was closely fulfilled at the design flow rates by his measurements. Higher spanwise gradients of axial velocity were present only near the nose cone and in the boundary layers on the nose cone and the casing wall.

Fig. 3 presents the pitch-averaged ideal total head rise coefficient, axial flow coefficient and radial flow coefficient profiles along the radius, which were calculated from the measured LDA data. During averaging, the ideal total head rise coefficient values were weighed with the axial flow coefficients.

Fig. 3 also displays characteristics of the theoretical flow, which was considered as an ideal flow pattern corresponding to the design concept based on two-dimensional stationary cascade data. The theoretical flow data serve as a basis for comparison between experiments and design theory for the flow outside the annulus wall boundary layers – termed the main flow. The design method by Somlyódy (1971) does not take the displacement effect of annulus wall boundary layers into account. Thus, although the flow rate was $\overline{\Phi}_D$ during the LDA measurements, distributions of $\hat{\psi}_{3D}(R)$ and $\hat{\varphi}_{3D}(R)$ could not be used for the main flow directly as theoretical flow data. $\hat{\psi}^*_3(R)$ and $\hat{\varphi}^*_3(R)$ in Fig. 3 derive from a slight correction of $\hat{\psi}_{3D}(R)$ and $\hat{\varphi}_{3D}(R)$ with the consideration of displacement effects. The correction method is not presented here, a summary can be found in Vad and Bencze (1996).

It is conspicuous in Fig. 3(a) that $\hat{\psi}^*_3(R)$ and $\hat{\psi}_3(R)$ agree well in the main flow only in the case of rotor BUP-29. Such good agreement cannot be observed between $\hat{\varphi}^*_3(R)$ and $\hat{\varphi}_3(R)$ even in the case of BUP-29 (Fig. 3(b)), which is due to the strong influence of annulus wall boundary layer displacement effects on the axial velocity profile. Nevertheless, theoretical and measured exit flow angle distributions (presented in Vad and Bencze, 1997) also showed the best (fair) agreement in the case of BUP-29. In addition, it was assumed that the inlet velocity profiles at $\overline{\Phi}_D$ are approximately identical for the three rotors. The above led eventually to the conclusion that blading BUP-29 is the most capable of realising the design conception concerning spanwise distributions of ideal total head rise as well as angle of turning. The adequate realisation of the design conception corresponds to an optimum cascade operation, which appears in the highest hydraulic efficiency of BUP-29 (see Section 3).

It can be seen in Fig. 3(c) that the pitch-averaged radial velocity profiles does not differ significantly in the main flow for the three rotors despite the different spanwise gradients of design ideal total head rise. According to the measurements reported here, $\hat{\varphi}_{r3}(R)$ can be estimated using a linear function:

$$\hat{\varphi}_{r3}(R) = \frac{K_{\varphi_r \max}}{R_{\max} - R_{\min}} (R - R_{\min}). \quad (2)$$

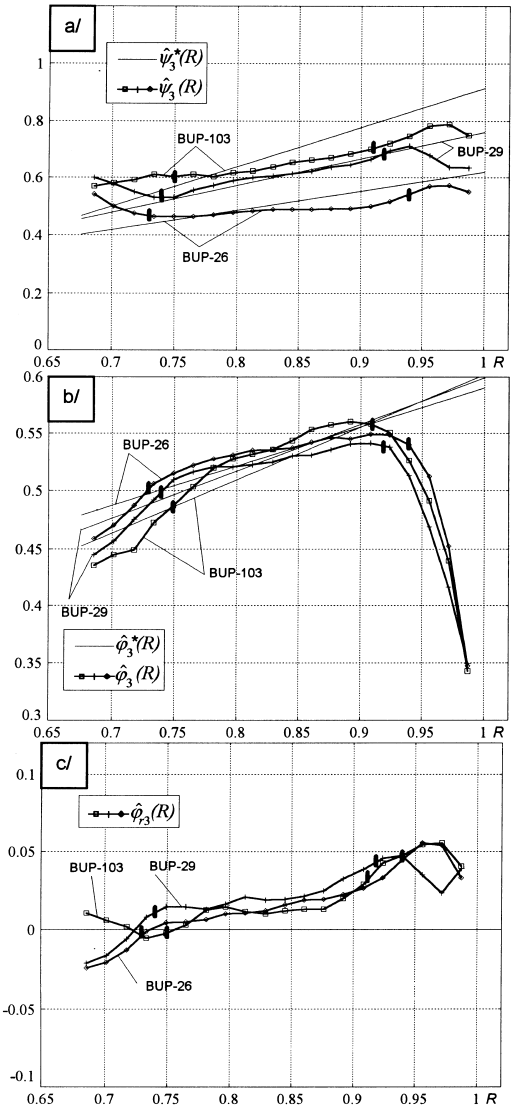

Fig. 3. Pitch-averaged data. (a) Ideal total head rise coefficient, (b) axial flow coefficient, (c) radial flow coefficient.

The approximation is valid within the main flow characterised by the radial range of $[R_{\min}, R_{\max}]$. $K_{\varphi_r \max} = 0.05$ for the rotors under present investigation. $R_{\min}$ and $R_{\max}$ can be estimated analysing diagrams of Fig. 3 and the secondary flow vector plots (see Section 4.2) simultaneously. The $R_{\min}$ and $R_{\max}$ values are marked in Fig. 3(a)–(c) by short bold bars. It can be observed that the annulus wall boundary layers thicken with increasing $\overline{\Psi}_t$ (see Fig. 2).

4.2. Secondary flow vector plots

To learn more about radial velocity components, pitchwise resolved flow data are also discussed. Vector plots of the secondary flow are shown in Fig. 4. Using the definition and calculation method of Inoue et al. (e.g. Inoue and Kuroumaru, 1984; Inoue et al., 1986), the secondary flow was obtained as a velocity component perpendicular to the relative theoretical flow direction.

Considering the relatively high hub-to-tip ratio and low blade pitch values, authors felt admissible to transform the annular sector measurement region into a rectangle during

representation. The plots are extended to a 40° angular range by means of copying the 6–11° section to the end of the measured range in order to get a better view of the flow structure.

The vortical NFVO flow pattern filling the largest part of the measurement range can be observed for each rotors with a single glance in Fig. 4. It consists of suction side outward (S) and pressure side inward (P) radial flow branches, linked with an overturning zone (O) near the hub and an underturning zone (U) near the casing wall. This paper does not concern the flow phenomena near the blade passage endwalls. Studies on the endwall boundary layers are presented e.g. in Vad and Bencze (1997).

To supply information for calculation on the torsion of stream surface segments, the tangential gradient of the radial velocity was characterised quantitatively. First, the centre of the NFVO flow was identified as a circular flow pattern of nearly zero secondary velocities (sign C in Fig. 4). The NFVO centre is forced slightly below midspan due to the dominant displacement effect of the casing wall boundary layer. However, it seemed to be reasonable for simplicity to model the NFVO flow as a vortical pattern centred at midspan. It was established hat there is a gapwise range existing between the

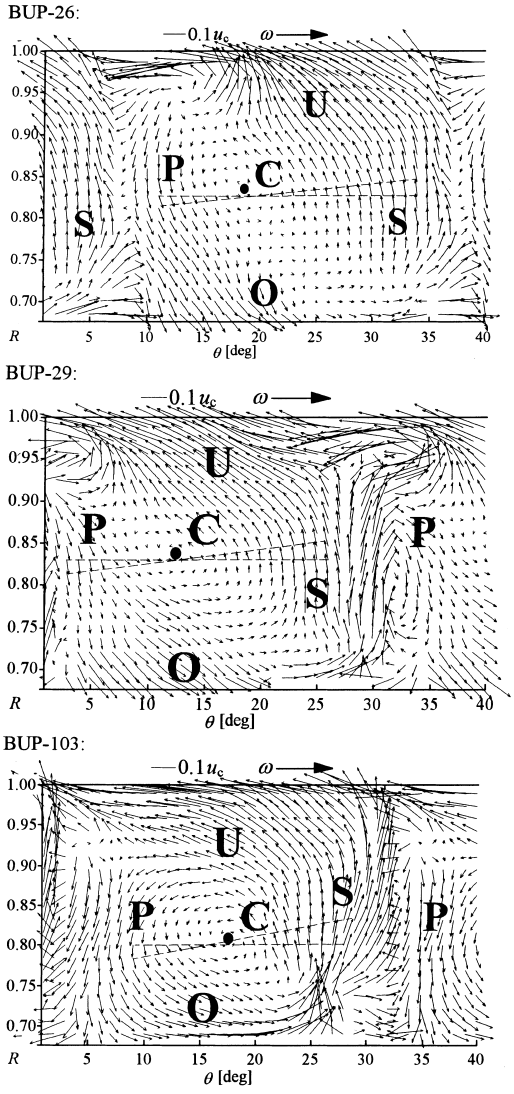

Fig. 4. Secondary flow vector plots.

Table 3
Gradients of radial velocity and design circulation

	$\frac{1}{R_{\mathrm{mid}}}\frac{\partial\varphi_{r3}}{\partial\theta}$	$\partial\hat{\psi}_{3D}/\partial R$	$\frac{1}{R_{\mathrm{mid}}}\frac{\partial\varphi_{r3}}{\partial\theta}/\partial\hat{\psi}_{3D}/\partial R$
BUP-26	0.291	0.771	**0.377**
BUP-29	0.350	1.043	**0.335**
BUP-103	0.495	1.343	**0.369**

blade wakes near the NFVO centre that can be characterised with approximately constant $(1/R_{\mathrm{mid}})(\partial\varphi_{r3}/\partial\theta)$ values (this tendency is marked with dashed lines in Fig. 4). Though Dring et al. (1982) also described a near linear gapwise variation of the radial velocity, their observation remained qualitative. In the present cases, representative $(1/R_{\mathrm{mid}})(\partial\varphi_{r3}/\partial\theta)$ values were calculated in such a way that the difference of the radial velocities at the endpoints of the dashed lines were divided by the corresponding arc length. $(1/R_{\mathrm{mid}})(\partial\phi_{r3}/\partial\theta)$ was found nearly in direct proportion with the midspan value of $\partial\hat{\psi}_{3D}/\partial R$, as shown in Table 3. This observation is summarised in the following relationship:

$$\frac{1}{R_{\mathrm{mid}}}\frac{\partial[\varphi_{r3}(R_{\mathrm{mid}})]}{\partial\theta} = K_r\frac{\partial\hat{\psi}_{3D}}{\partial R}(R_{\mathrm{mid}}), \tag{3}$$

where K_r is dependent upon the blade number N. Averaging the bold values in Table 3, $K_r = 0.36$ was established for the rotors under present investigation. It can be seen in Fig. 4 that the maximum value of $\partial\varphi_{r3}/\partial\theta$ appears near midspan which means that a maximum torsion of stream surface segments is also expected at R_{mid}. Therefore, the model in Eq. (3) gives an aid for pessimistic calculations on stream surface torsion.

4.3. Torsion of stream surface segments

In the following calculations, the stream surface segments were modelled at midspan as surfaces twisted directly behind the leading edges and then remaining plane within the blade passages and parallel to the duct axis. This model enables the characterisation of the torsion of stream surfaces at midspan by the angle between circumferential direction and the above mentioned plane surfaces. The NFVO flow is approximated in the rotor exit plane as a vortex of solid body rotation centred at midspan and midpitch (Fig. 5). This means that the pitch-averaged radial velocity at midspan (which represents a radial translation of the stream surface segment) is neglected in the calculations discussed below.

Using Eq. (3), the radial flow coefficient in the rotor exit plane at midspan at a location characterised by θ can be calculated as follows:

$$\varphi_{r3}(R_{\mathrm{mid}},\theta) = K_r R_{\mathrm{mid}}\,\theta\frac{\partial\hat{\psi}_{3D}}{\partial R}. \tag{4}$$

The average time during which a fluid element passes through the blade passage is approximately

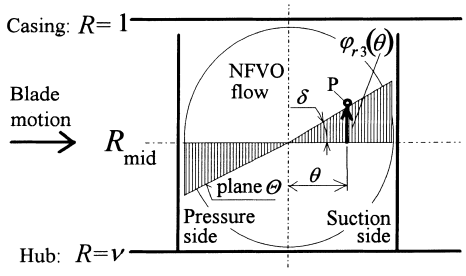

Fig. 5. NFVO flow model in the rotor exit plane.

$$T = \ell/\hat{w}_\infty(R_{\mathrm{mid}}) \tag{5}$$

for which the relative design mean velocity $\hat{w}_\infty(R_{\mathrm{mid}})$ is calculated in the following way:

$$\hat{w}_\infty(R_{\mathrm{mid}}) = u_c \left[\left(\frac{\overline{\Phi}_D + \hat{\varphi}_{3D}(R_{\mathrm{mid}})}{2} \right)^2 + \left(R_{\mathrm{mid}} - \frac{\hat{\psi}_{3D}(R_{\mathrm{mid}})}{4R_{\mathrm{mid}}} \right)^2 \right]^{1/2}. \tag{6}$$

If a fluid element enters the blade passage at midspan and leaves it at point P (Fig. 5), its radial co-ordinate deviates from R_{mid} with ΔR, where ΔR can be calculated by substituting Eqs. (4) and (5) into the following equation:

$$\Delta R = \varphi_{r3}(R_{\mathrm{mid}}, \theta) T \omega. \tag{7}$$

The torsion angle δ (Fig. 5) is obtained using Eq. (7)

$$\delta = \tan^{-1}[\Delta R/(R_{\mathrm{mid}}\theta)]. \tag{8}$$

The calculated δ values are shown in Table 4.

If straight (unswept) blades are designed, the stream surface torsion could be taken into account in the following way. The twisted plane stream surface segment Θ (Fig. 5) crosses the neighbouring blades approximately at radii $R_- = R_{\mathrm{mid}}[1 - (\pi/N)\tan\delta]$ and $R_+ = R_{\mathrm{mid}}[1 + (\pi/N)\tan\delta]$. For the calculation of the blade geometry at R_{mid}, representative design parameters $\hat{\psi}_{3D\,\mathrm{repr}}(R_{\mathrm{mid}})$ and $\hat{\varphi}_{3D\,\mathrm{repr}}(R_{\mathrm{mid}})$ are assumed to be obtained in such a way that the original parameter values $\hat{\psi}_{3D}(R_-), \hat{\psi}_{3D}(R_+)$ and $\hat{\varphi}_{3D}(R_-), \hat{\varphi}_{3D}(R_+)$ are simply averaged in pairs. Considering that the $\hat{\psi}_{3D}(R)$ and $\hat{\varphi}_{3D}(R)$ distributions have been linearised, the averaging operations result that $\hat{\psi}_{3D\,\mathrm{repr}}(R_{\mathrm{mid}}) = \hat{\psi}_{3D}(R_{\mathrm{mid}})$ and $\hat{\varphi}_{3D\,\mathrm{repr}}(R_{\mathrm{mid}}) = \hat{\varphi}_{3D}(R_{\mathrm{mid}})$. This would generally mean that the torsion of the stream surface segments do not play a role from the design point of view. The acceptance of the above train of thought is obviously limited corresponding to the extent of change of $\hat{\psi}_{3D}$ and $\hat{\varphi}_{3D}$ parameters within the range $[R_-; R_+]$. Table 4 summarises the changes within $[R_-; R_+]$ relative to the values at midspan.

It is assumed that the neglect of stream surface torsion is a necessary condition for the success of using two-dimensional cascade data in NFV design. It is undoubted that the design method was the most successful in the case of rotor BUP-29 (refer to the former observations regarding Figs. 2 and 3). Therefore, the following conclusion can be made based on data in Table 4: the torsion of stream surface segments is negligible from the design point of view if

$$\left| \frac{\hat{\psi}_{3D}(R) - \hat{\psi}_{3D}(R_{\mathrm{mid}})}{\hat{\psi}_{3D}(R_{\mathrm{mid}})} \right| \leqslant 0.10 \tag{9a}$$

and in addition,

$$\left| \frac{\hat{\varphi}_{3D}(R) - \hat{\varphi}_{3D}(R_{\mathrm{mid}})}{\hat{\varphi}_{3D}(R_{\mathrm{mid}})} \right| \leqslant 0.05 \tag{9b}$$

within the calculated $[R_-; R_+]$ range. In the cases when conditions (9a) and (9b) are fulfilled, the assumption of stream surfaces of revolution through the rotor is confirmed.

Table 4
Results of stream surface torsion analysis

	δ/deg	$\left\lvert\frac{\hat{\psi}_{3D}(R)-\hat{\psi}_{3D}(R_{\mathrm{mid}})}{\hat{\psi}_{3D}(R_{\mathrm{mid}})}\right\rvert$	$\left\lvert\frac{\hat{\varphi}_{3D}(R)-\hat{\varphi}_{3D}(R_{\mathrm{mid}})}{\hat{\varphi}_{3D}(R_{\mathrm{mid}})}\right\rvert$
BUP-26	8.0	max 0.04	max 0.02
BUP-29	14.3	max 0.10	max 0.05
BUP-103	21.4	max 0.20	max 0.11

In order to refine the above calculations, data should be obtained on the formation of stream surfaces within the blading. For this purpose, throughflow computations will be carried out in the near future using the XENIOS three-dimensional turbulent finite element code (e.g. Borello et al., 1997).

4.4. Blade geometry calculations with the consideration of the pitch-averaged radial velocity

It has been concluded in the previous section that stream surfaces of revolution can be presumed within the blading if conditions (9a) and (9b) are fulfilled. It was expected that the optimum behaviour of rotor BUP-29 can be justified through blade calculations with taking the pitch-averaged radial velocity appropriately into account. Calculations were carried out to satisfy this need. Since these calculations are rather lengthy to be described, only a short summary is given here on them. Their full description can be found in Vad (1997).

It was assumed that the radial velocity distribution modelled in Eq. (2) forms directly behind the leading edges and it remains constant through the rotor. In addition, the axial flow at an arbitrary radius R through the rotor was taken into account with the constant mean value of design axial velocities upstream and downstream of the rotor: $\hat{\varphi}_{03D}(R) = (\overline{\Phi}_D + \hat{\varphi}_{3D}(R))/2$. Thus, the stream surfaces were modelled as cones of half-angle $\alpha_{\mathrm{cone}} = \tan^{-1}(\hat{\varphi}_{r3}/\hat{\varphi}_{03D})$. The cones were assumed to extend along the duct axis from leading to trailing edges of the blades. The inlet and outlet radii of the cones have been calculated.

Using two-dimensional cascade data, the NFV design was considered in such a way that the blades are swept and the blade sections calculated using two-dimensional cascade data fit onto the conical stream surfaces, forming "elemental rotors". The law of moment of momentum was applied to the fluid within the elemental rotors enclosed by rotor inlet and exit planes and two neighbouring conical surfaces. On the other hand, the torque appropriate to each of the elemental rotors was expressed from the aerodynamic forces acting on the blades. From these two equations, force factor $(\ell/t)c_{\mathrm{lift}}$ was calculated. The optimum ℓ/t, chamber radius of curvature and γ cascade characteristics were calculated using the classic method (Howell et al., 1945; Wallis, 1961). Since the blade sweep was found negligible, the results are fully informative in the design of straight blades.

The calculations showed that taking the pitch-averaged radial velocity into account leaves the γ values nearly unchanged and makes a 3–8% reduction in the chamber radius of curvature. The most interesting results regard ℓ/t solidity values. Fig. 6 shows the realised ℓ/t solidities and solidities calculated for radii out of the annulus wall boundary layers, without and with the above consideration of the radial velocity. The reader is reminded now that the realised solidity values differ from the original design values.

Fig. 6 shows that the realised solidities at radii $0.85 < R < 0.90$ are relatively the closest in the case of rotor BUP-29 to the ℓ/t values obtained with the consideration of the radial velocity component. It can be also observed in Fig. 3(a) that at radii $0.85 < R < 0.92$ the agreement is very good between $\hat{\psi}_3^*(R)$ and $\hat{\psi}_3(R)$ for rotor BUP-29. The theoretical and realised exit flow angles agree the best in this R range also in the case of BUP-29 (see Vad and Bencze, 1997). This suggests that taking the radial velocity into account is advantageous from the viewpoint of the realisation of NFV design conception. It must be also noted here that the proper realisation of the design conception is especially important at these high radii since the airfoils near the circumference contribute to a greater extent to the rotor performance, due to the high ideal total

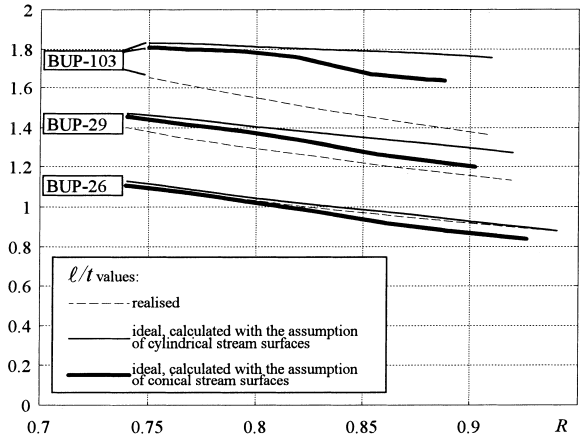

Fig. 6. Solidity distributions.

head rise prescribed for them. This explains why BUP-29 could perform a relatively high $\overline{\Psi}_t$ (see Fig. 2).

5. Conclusions

Three-dimensional LDA measurements were carried out downstream of isolated axial fan rotors of non-free vortex design. The aim of the measurements was to supply information on the radial velocity component developing in the rotors and to give instructions for taking the radial velocity component into account in design. The results are summarised as follows.

1. The pitch-averaged radial velocity profile remains nearly unchanged at the rotor exit as the spanwise gradient of design ideal total head rise increases. It can be modelled in design with a linear function (Eq. (2)).
2. The tangential gradient of radial velocity at midspan at the rotor exit is approximately in direct proportion with the spanwise gradient of design ideal total head rise (Eq. (3)).
3. The torsion of stream surface segments is negligible in design if conditions (9a) and (9b) are fulfilled. These conditions summarise the limitations in the spanwise change of design local ideal total head rise and design local flow rate.
4. Taking the pitch-averaged radial velocity into account in design with the assumption of conical stream surfaces through the rotor has the following advantages: (i) the spanwise distribution of design ideal total head rise is realised more accurately and a higher total head rise is performed by the rotor, (ii) the rotor hydraulic efficiency is improved.

Acknowledgements

The experimental work was supported financially by OTKA (Hungarian National Foundation for Science and Research) under contract T 16950.

References

Bencze, F., Szlivka, F., 1987. A new method for the design of axial flow fans of changing circulation. Eighth Conference on Fluid Machinery, Budapest.

Borello, D., Corsini, A., Rispoli, F., 1997. Prediction of francis turbine runner performance using a 3D finite element technique with unassembled stiffness matrix treatment. Second European Conference on Turbomachinery, Fluid Dynamics and Thermodynamics, Antwerpen, Belgium.

Briley, N.R., McDonald, H., 1979. Analysis and computation of viscous subsonic primary and secondary flows. Fourth AIAA Computational Fluid Dynamics Conference, Williamsburg.

Caspar, J.R., Hobbs, D.E., Davis, R.L., 1980. Calculation of two-dimensional potential cascade flow using finite area methods. AIAA Journal 18 (1), 103–109.

Dodge, P.R., 1976. A numerical method for two- and three-dimensional viscous flows. AIAA Paper No. 76–425, AIAA nineth Fluid and Plasma Dynamics Conference, San Diego.

Dring, R.P., Joslyn, H.D., Hardin, L.W., 1982. An investigation of axial compressor rotor aerodynamics. ASME Journal of Engineering for Power 104, 84–96.

Goto, A., 1992. Three-dimensional flow and mixing in an axial flow compressor with different tip clearances. ASME Journal of Turbomachinery 114, 675–685.

Howell, A.R., 1942. The present basis of axial flow compressor design. Part. I, Cascade Theory and Performance, Aeronautical Research Council R. and M. 2095, London, UK.

Howell, A.R., Mettam, M., Nock, J., 1945. Some general notes on axial flow compressor design. Power Jets Report R 1088.

Inoue, M., Kuroumaru, M., 1984. Three-dimensional structure and decay of vortices behind an axial flow rotating blade row. ASME Journal of Engineering for Gas Turbines and Power 106, 561–569.

Inoue, M., Kuroumaru, M., Fukuhara, M., 1986. Behavior of tip leakage flow behind an axial compressor rotor. ASME Journal of Engineering for Gas Turbines and Power 108, 7–14.

Meixner, H.U., 1994. Vergleichende LDA-Messungen an ungesichelten und gesichelten axialventilatoren. Ph.D. Thesis, University of Karlsruhe, Germany.

Somlyódy, L., 1971. Berechnung der Beschaufelung und der Strömung axial durchströmter Wirbelmaschinen mit Anwendung von Gittermessung. Periodica Polytechnica, No. 3. Budapest.

Vad, J., Bencze, F., Füredi, G., Szombati, R., 1995. Fluid mechanical investigation on axial flow fans. Tenth Conference on Fluid Machinery, Budapest, pp. 500–509.

Vad, J., Bencze, F., 1996. Secondary flow in axial flow fans of non- free vortex operation. Eighth International Symposium on Applications of Laser Techniques to Fluid Mechanics, Lisbon, Portugal. 1 pp. 14.6.1–14.6.8.

Vad, J., 1997. Investigation on the flow field downstream of axial flow fans using laser doppler anemometry. Ph.D. Thesis, Technical University of Budapest, Hungary.

Vad, J., Bencze, F., 1997. Casing wall boundary layer flow in axial flow fans of non-free vortex design. Submitted to ASME Journal of Fluids Engineering, Log No. 4780-BS.

Wagner, J.H., Dring, R.P., Joslyn, H.D., 1985. Inlet boundary layer effects in an axial compressor rotor. Parts I-II, ASME Journal of Engineering for Gas Turbines and Power 107.

Wallis, R.A., 1961. Axial Flow Fans. Newnes, London.

Wu, C.H., 1952. A general theory of three-dimensional flow in subsonic and supersonic turbomachines of axial, radial and mixed-flow types, Transactions of the ASME 74 (8).